REPORT DOCUMENTATION PAGE

Form Approved OMB NO. 0704-0188

1. REPORT DATE (DD-MM-YYYY)	2. REPORT TYPE	3. DATES COVERED (From - To)
09-01-2016	Final Report	10-Sep-2012 - 9-Oct-2015

4. TITLE AND SUBTITLE

Final Report: Research Topic Area 10.4: Physical Properties of Materials: Epitaxial Semiconducting Heusler Alloy Heterostructures

5a. CONTRACT NUMBER
W911NF-12-1-0459

5b. GRANT NUMBER

5c. PROGRAM ELEMENT NUMBER
611102

6. AUTHORS

Chris Palmstrom

5d. PROJECT NUMBER

5e. TASK NUMBER

5f. WORK UNIT NUMBER

7. PERFORMING ORGANIZATION NAMES AND ADDRESSES

University of California - Santa Barbara
3227 Cheadle Hall
3rd floor, MC 2050
Santa Barbara, CA 93106 -2050

8. PERFORMING ORGANIZATION REPORT NUMBER

9. SPONSORING/MONITORING AGENCY NAME(S) AND ADDRESS (ES)

U.S. Army Research Office
P.O. Box 12211
Research Triangle Park, NC 27709-2211

10. SPONSOR/MONITOR'S ACRONYM(S)
ARO

11. SPONSOR/MONITOR'S REPORT NUMBER(S)
62176-MS.7

12. DISTRIBUTION AVAILIBILITY STATEMENT

Approved for Public Release; Distribution Unlimited

13. SUPPLEMENTARY NOTES

The views, opinions and/or findings contained in this report are those of the author(s) and should not contrued as an official Department of the Army position, policy or decision, unless so designated by other documentation.

14. ABSTRACT

Molecular beam epitaxy has been used to successfully grow high quality single crystal films of semiconducting half-Heusler compounds on lattice matched conventional compound semiconductor heterostructures. The atomic surface reconstruction and electronic properties were studied in detail using scanning tunneling microscopy and angle resolved photoemission. For the doping levels achieved in cobalt titanium antimony, the electron mobility at room temperature was comparable to those of silicon. X-ray photoelectron spectroscopy was used to determine the electronic valence band alignment between cobalt titanium antimony and indium gallium arsenide and aluminum

15. SUBJECT TERMS

Epitaxial Growth, MBE, Heusler Alloys, Heusler compounds, semiconductors, topological

16. SECURITY CLASSIFICATION OF:			17. LIMITATION OF ABSTRACT	15. NUMBER OF PAGES	19a. NAME OF RESPONSIBLE PERSON
a. REPORT	b. ABSTRACT	c. THIS PAGE			Christopher Palmstrom
UU	UU	UU	UU		19b. TELEPHONE NUMBER 805-893-3618

Report Title

Final Report: Research Topic Area 10.4: Physical Properties of Materials: Epitaxial Semiconducting Heusler Alloy Heterostructures

ABSTRACT

Molecular beam epitaxy has been used to successfully grow high quality single crystal films of semiconducting half-Heusler compounds on lattice matched conventional compound semiconductor heterostructures. The atomic surface reconstruction and electronic properties were studied in detail using scanning tunneling microscopy and angle resolved photoemission. For the doping levels achieved in cobalt titanium antimony, the electron mobility at room temperature was comparable to those of silicon. X-ray photoelectron spectroscopy was used to determine the electronic valence band alignment between cobalt titanium antimony and indium gallium arsenide and aluminum gallium arsenide suggesting that it may make an excellent ohmic contact to n-type materials. Controlled alloying with nickel titanium antimony allowed controlled electron doping, resulting in metallic behavior for alloy concentrations above 20%. The predicted topological compound platinum lutetium antimonide was grown on indium aluminum antimony using molecular beam epitaxy. Integrated and spin polarized angle resolved photoemission studies were used to measure a Dirac-like linear dispersing surface state with helical spin texture. The results are a direct measure of the predicted topological surface state, confirming platinum lutetium antimony to be a topological material.

Enter List of papers submitted or published that acknowledge ARO support from the start of the project to the date of this printing. List the papers, including journal references, in the following categories:

(a) Papers published in peer-reviewed journals (N/A for none)

Received		Paper
01/08/2016	4.00	Sahil J. Patel, John A. Logan, Sean D. Harrington, Brian D. Schultz, Chris J. Palmstrøm. Surface reconstructions and transport of epitaxial PtLuSb (001) thin films grown by MBE, Journal of Crystal Growth, (02 2016): 0. doi: 10.1016/j.jcrysgro.2015.12.003
08/29/2013	1.00	Jason K. Kawasaki, Thomas Neulinger, Rainer Timm, Martin Hjort, Alexei A. Zakharov, Anders Mikkelsen, Brian D. Schultz, Chris J. Palmstrøm. Epitaxial growth and surface studies of the Half Heusler compound NiTiSn (001), Journal of Vacuum Science & Technology B: Microelectronics and Nanometer Structures, (07 2013): 41060. doi: 10.1116/1.4807715
08/30/2014	2.00	Jason K. Kawasaki, Linda I. M. Johansson, Brian D. Schultz, Chris J. Palmstrøm. Growth and transport properties of epitaxial lattice matched half Heusler CoTiSb/InAlAs/InP(001) heterostructures, Applied Physics Letters, (01 2014): 0. doi: 10.1063/1.4862191
TOTAL:	**3**	

Number of Papers published in peer-reviewed journals:

(b) Papers published in non-peer-reviewed journals (N/A for none)

Received	Paper

TOTAL:

Number of Papers published in non peer-reviewed journals:

(c) Presentations

Plenary Talk: International MBE Conference, Nara, Japan, Sept 23-28, 2012, "Dissimilar materials epitaxy: from layered heterostructures to nanocomposites", C. J. Palmstrøm

Plenary Talk: 32nd International Conference on the Physics of Semiconductors, Austin, Texas, August 10-15, 2014, “Integration of Heusler Compounds with III-V Semiconductors: Semiconductor Spintronics and More", C. J. Palmstrøm

Plenary Talk: AVS Topical Conference, 2015 Shanghai Thin Film Conference, October 24-25, 2015, “Molecular Beam Epitaxial Growth of Spintronic Materials”, C.J. Palmstrøm

Invited Talk: AVS 60th International Symposium and Exhibition, Long Beach, CA, October 27-November 1, 2013, "Why all the Interest in Heusler Alloys?", C. J. Palmstrøm

Invited Talk: 2015 Lawrence Workshop on Epitaxy, Tempe, AZ, February 26-27, 2015, “Heusler Compounds on III-V Semiconductors: growth, surfaces, interfaces and electronic structure", C. J. Palmstrøm

Invited Talk: NAMBE 2015 (MBE Innovator Award Presentation): "MBE Growth of Dissimilar Materials", C. J. Palmstrøm

Invited talk: AVS 2013: “Epitaxial Growth and Electronic Bandstructure of the Semiconducting Half Heusler Compound CoTiSb”, J. Kawasaki, L. Johansson, M. Hjort, R. Timm, B. Shojaei, A. Mikkelsen, B.D. Schultz, and C. Palmstrøm

Contributed Talks:

NAMBE 2013: "Epitaxial growth, transport, and electronic structure of Half Heusler compounds: CoTiSb, NiTiSn, and Ni2TiSn:NiTiSn nano composite films", J. K. Kawasaki, L. M. Johansson, J. Shabani, S. Patel, A. Rice, M. Hjort, R. Timm, B. D. Schultz, T. Balasubramanian, A. Mikkelsen, and C. J. Palmstrøm

MRS 2013: "Epitaxial growth, transport, and electronic structure of the Half Heusler compounds CoTiSb and NiTiSn", J.K. Kawasaki, L. M. Johansson, A. Rice, R. Timm, M. Hjort, A. Mikkelsen, and C. J. Palmstrøm

APS March Meeting 2013: “Electronic band structure, doping, and defects in the semiconducting Half Heusler compound CoTiSb”, J. K. Kawasaki, L. M. Johansson, M. Hjort, R. Timm, B. D. Schultz, T. Balasubramanian, A. Mikkelsen, and C. J. Palmstrøm

AVS 2013: “Epitaxial Growth, Transport, and Electronic Structure of Half Heusler Compounds: CoTiSb, NiTiSn, and Ni2TiSn/NiTiSn Nanocomposite Films”, J.K. Kawasaki, L.M. Johansson, J. Shabani, A. Rice, M. Hjort, R. Timm, B.D. Schultz, T. Balasubramanian, A. Mikkelsen, and C.J. Palmstrøm

PCSI-42 2015: "Surface and Electronic Structure of half-Heusler PtLuSb (001) Thin-Films Grown by Molecular Beam Epitaxy", J. A. Logan, S. J. Patel, S. D. Harrington, J. K. Kawasaki, B. D. Schultz, A. Mikkelsen and C. J. Palmstrøm

PCSI-42 2015: "Epitaxial growth and electronic structure of half Heusler Co1-xNixTiSb", S. D. Harrington, J. A. Logan, S. J. Patel, J. K. Kawasaki, T. Balasubramanian, A. Mikkelsen, and C. J. Palmstrøm

Number of Presentations: 13.00

Non Peer-Reviewed Conference Proceeding publications (other than abstracts):

Received Paper

TOTAL:

Number of Non Peer-Reviewed Conference Proceeding publications (other than abstracts):

Peer-Reviewed Conference Proceeding publications (other than abstracts):

Received	Paper

TOTAL:

Number of Peer-Reviewed Conference Proceeding publications (other than abstracts):

(d) Manuscripts

Received	Paper	
01/08/2016	5.00	John Logan, Sahil Patel, Sean Harrington, Craig Polley, Brian Schultz, Thiagarajan Balasubramanian, Anderson Janotti, Anders Mikkelsen, Chris Palmstrøm. Observation of a topologically non-trivial surface state in half-Heusler PtLuSb (001) thin films, Nature Communications (11 2015)

TOTAL: **1**

Number of Manuscripts:

Books

Received	Book

TOTAL:

Received	Book Chapter

TOTAL:

Patents Submitted

Patents Awarded

Awards

Chris Palmstrøm: 2015 NAMBE MBE Innovator Award
Chris Palmstrøm: 2015 DOD-National Security Science and Engineering Fellow
Jason Kawasaki: 2013 AVS-MIND Leo-Falicov-Student Award winner
Jason Kawasaki: 2013 AVS Russell & Sigurd Varian Award winner

Graduate Students

NAME	PERCENT_SUPPORTED	Discipline
Jason Kawasaki	0.50	
Borzoyeh Shojaei	0.01	
John Logan	1.00	
Sean Harrington	0.50	
Tobias Brown-Heft	0.08	
Ryan Need	0.05	
Sahil Patel	0.30	
FTE Equivalent:	**2.44**	
Total Number:	**7**	

Names of Post Doctorates

NAME	PERCENT_SUPPORTED
FTE Equivalent:	
Total Number:	

Names of Faculty Supported

NAME	PERCENT_SUPPORTED	National Academy Member
Chris Palmstrom	0.08	
FTE Equivalent:	**0.08**	
Total Number:	**1**	

Names of Under Graduate students supported

NAME	PERCENT_SUPPORTED
FTE Equivalent:	
Total Number:	

Student Metrics

This section only applies to graduating undergraduates supported by this agreement in this reporting period

The number of undergraduates funded by this agreement who graduated during this period:	0.00
The number of undergraduates funded by this agreement who graduated during this period with a degree in science, mathematics, engineering, or technology fields:.....	0.00
The number of undergraduates funded by your agreement who graduated during this period and will continue to pursue a graduate or Ph.D. degree in science, mathematics, engineering, or technology fields:.....	0.00
Number of graduating undergraduates who achieved a 3.5 GPA to 4.0 (4.0 max scale):.....	0.00
Number of graduating undergraduates funded by a DoD funded Center of Excellence grant for Education, Research and Engineering:.....	0.00
The number of undergraduates funded by your agreement who graduated during this period and intend to work for the Department of Defense	0.00
The number of undergraduates funded by your agreement who graduated during this period and will receive scholarships or fellowships for further studies in science, mathematics, engineering or technology fields:	0.00

Names of Personnel receiving masters degrees

NAME
Total Number:

Names of personnel receiving PHDs

NAME	
Jason Kawasaki	
Sahil Patel	
Total Number:	**2**

Names of other research staff

NAME	PERCENT_SUPPORTED
Brian Schultz	0.10
FTE Equivalent:	**0.10**
Total Number:	**1**

Sub Contractors (DD882)

Inventions (DD882)

Scientific Progress

Technology Transfer

Discussions with Patrick Folkes (RDCOM ARL) on initiating collaborations on Topological Heusler compounds
Discussions with Chip Eddy (NRL) on initiating collaborations on epitaxial growth at low temperatures
Discussions with Joe Tischler (NRL) on optical properties of Heusler compounds

Interactions with Jerry Tersoff (IBM) - discussions on viability of Heusler alloys
Discussions with Kurt Eyink AFRL on metal-semiconductor composites

ARO W911NF-12-1-0459
Final Report 08/01/12-07/31/15

Epitaxial growth and electronic structure of half Heuslers $Co_{1-x}Ni_xTiSb$ (001), $Ni_{1-x}Co_xTiSn$, and PtLuSb

Chris J. Palmstrøm

Department of Electrical & Computer Engineering and Materials Department
University of California, Santa Barbara CA 93106

Abstract

Molecular beam epitaxy has been used to successfully grow high quality single crystal films of semiconducting half-Heusler compounds on lattice matched conventional compound semiconductor heterostructures. The atomic surface reconstruction and electronic properties were studied in detail using scanning tunneling microscopy and angle resolved photoemission. For the doping levels achieved in cobalt titanium antimony, the electron mobility at room temperature was comparable to those of silicon. X-ray photoelectron spectroscopy was used to determine the electronic valence band alignment between cobalt titanium antimony and indium gallium arsenide and aluminum gallium arsenide suggesting that it may make an excellent ohmic contact to n-type materials. Controlled alloying with nickel titanium antimony allowed controlled electron doping, resulting in metallic behavior for alloy concentrations above 20%. The predicted topological compound platinum lutetium antimonide was grown on indium aluminum antimony using molecular beam epitaxy. Integrated and spin polarized angle resolved photoemission studies were used to measure a Dirac-like linear dispersing surface state with helical spin texture. The results are a direct measure of the predicted topological surface state, confirming platinum lutetium antimony to be a topological material.

Table of Content

Introduction

Half Heusler compounds are an exciting class of intermetallics due to their multifarious electrical and magnetic properties, including semiconducting[1], half metallic[2], and thermoelectric[3] behaviors. Additionally, a number of the half Heusler compounds have been predicted to be topological insulators [4]. Half-Heusler materials have similar crystal structure and lattice parameters as III-V compound semiconductors, suggesting the possibility of half-Heusler/III-V semiconductor heterostructures with unique properties. In particular, the semiconducting half-Heusler compound CoTiSb, predicted to have ~1 eV band gap[1], has been extensively studied in the bulk and recently in films grown by molecular beam epitaxy (MBE) where record high carrier mobilities were demonstrated [5]. In contrast, NiTiSb, which has one more valence electron per formula unit, displays metallic behavior. By substitutionally alloying Ni on the Co site, the electronic band structure can be tuned.

During the grant duration we have investigated the growth and electronic structure of semiconducting half Heusler films grown by MBE. In particular, the growth conditions of CoTiSb which minimize crystal defects were explored, yielding carrier concentrations and mobilities comparable to n-type Si with similar doping at room temperature. The periodicity, composition, bonding, and real space atomic positions at the CoTiSb (001) surface were determined. Additionally, the semiconductor to metal transition in $Co_{1-x}Ni_xTiSb$ (001) films as a function of Ni concentration was examined using electrical transport, Seebeck, and angle-resolved photoemission spectroscopy (ARPES) measurements. A cross over from semiconducting to metallic behavior was observed for films with greater than 10% Ni alloying. X-ray photoemission spectroscopy (XPS) was used to measure the valence-band offset ΔE_v between the semiconducting half Heusler, CoTiSb, and the lattice-matched III-V compound semiconductors, $In_{0.53}Ga_{0.47}As$ and $In_{0.52}Al_{0.48}As$. The electrical properties of CoTiSb/NiTiSn heterostructures were also measured. Finally, the surface states in the topological insulator candidate, PtLuSb, were examined using spin integrated and spin-resolved ARPES.

Results

CoTiSb Studies

CoTiSb films were grown on InAlAs buffer layers grown on semi-insulating InP:Fe (001) substrates to enable in-plane electrical transport measurements. CoTiSb was grown by simultaneous deposition from elemental Co, Ti, and Sb effusion cell sources using stoichiometric fluxes calibrated by *ex-situ* Rutherford backscattering spectrometry. It was found that for nucleation above 360 °C, the RHEED pattern begins to lose intensity, presumably due to reactions at the CoTiSb/InAlAs interface. To minimize this interfacial reaction, two approaches were employed. The first approach was to grow a lower temperature seed layer of CoTiSb at 260 °C for a few nm, then anneal and continue CoTiSb growth at a higher temperature. As bulk diffusion will be much slower than surface diffusion during growth, the interfacial reactions should be substantially reduced using this lower temperature initiation layer. Using this seed layer approach, CoTiSb has been grown at temperatures up to 460 °C without a significant reduction of the RHEED intensity. For all growths using stoichiometric fluxes and substrate temperatures within the range 260 – 460 °C, the (2×1)

surface reconstruction is observed. The second approach was to grow a thin ErAs diffusion barrier between CoTiSb and the InAlAs layers**.** This approach has been used previously for the growth of highly reactive transition metal alloys on III-Vs.[34,35] With the ErAs diffusion barrier, growth directly on ErAs has been performed at temperatures in excess of 510 °C without a substantial reduction in intensity of the RHEED pattern.

Figure 1 shows temperature dependent transport measurements for a 30 nm CoTiSb film on InAlAs/InP(001) grown using the seed layer approach (260 °C seed and 410 °C continued growth). As the measurement temperature increases from 2 to 300 K the zero field resistivity decreases consistent with semiconducting-like transport and thermally activated behavior. When replotted in Arrhenius form (Figure 1(b) insert, logarithm of n_H versus $1/k_BT$) the temperature dependent Hall carrier density shows three distinct regions upon cooling – a decrease in density from room temperature to 64 K ($1/k_BT$ < 180 eV^{-1}), a plateau from 64 to 43 K (180 to 270 eV^{-1}), and a decrease below 43 K (> 290 eV^{-1}) – that are reminiscent of the intrinsic, saturation, and freeze-out (or localization) expected for heavily doped semiconductors. In the high temperature region (< 180 eV^{-1}), although 300 K is not quite high enough to approach the expected n ~ exp(-E_g/2kT) dependency for intrinsic behavior and activation across the bandgap, from a fit in the range 240 - 300 K we estimate a lower bound for the bandgap of E_g > 0.13 eV. This is considerably smaller than the DFT bandgap of 1 eV,[18] which is suggestive that defect states rather than the intrinsic band gap is responsible for the thermally activated transport. Further reduction in electronically active defects is required to determine the true bandgap using transport measurements.

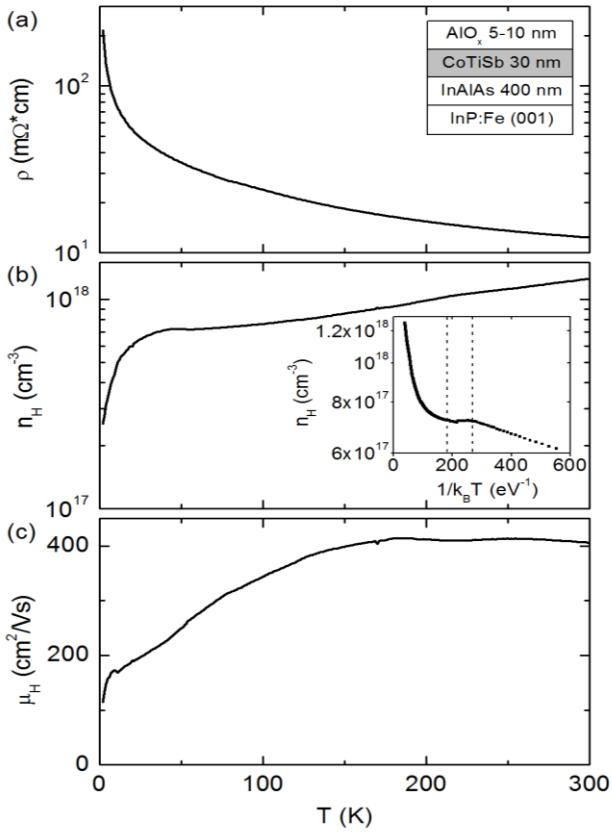

Figure 1 Temperature dependent transport measurements for a 30 nm CoTiSb film on InAlAs/InP. (a) Zero field resistivity. (b) and (c) plot the single carrier Hall density (n-type) and mobility extracted from Rxy at B = ± 1 T. The insert of (b) shows the density replotted in logarithmic scale versus 1/kBT.

In order to visualize the surface reconstructions in real space, *in-situ* room temperature STM measurements were performed on each of the reconstructions. Figure 2(a) shows a 30×30 nm filled states STM image of a (2×1)/*c*(2×4) terminated CoTiSb film grown on ErAs/InAlAs/InP. Since ErAs is 4-fold rotationally symmetric, mixed rotational domains of both (2×1)/(1×2) and c(2×4)/*c*(4×2) are observed where the (1×2) and *c*(4×2) are rotated from the (2×1) and *c*(2×4) respectively by 90 degrees. A number of steps are observed on this surface, each with a height of 2.9 Å = a_0/2, which corresponds to the spacing between Ti-Sb/Ti-Sb

planes. All step edges are <110> type and are predominantly (2×1) terminated, suggesting that (2×1) edge terminations are energetically more favorable than *c*(2×4) edge terminations.

Figure 2(b) shows a magnified filled states STM image in which both *c*(2×4) and (2×1) unit cells are resolved. No clear dependence on sample bias in the range -1.5 to +1.5 V was observed. Both reconstructions are characterized by structures with a periodicity of 8.3 Å along [-110], or twice the bulk-spaced unit cell, which are the length and direction expected for surface Sb dimers. Additionally, there is no step height variation between the two domains.

$Co_{1-x}Ni_xTiSb$ Alloy Studies

$Co_{1-x}Ni_xTiSb$ samples were grown in a VG V80 MBE system on lattice-matched $In_{0.52}Al_{0.48}As$ or $In_{0.53}Ga_{0.47}As$ buffers on InP (001) substrates[5]. For electrical transport measurements, an undoped InAlAs buffer on semi insulating InP:Fe (001) was used. For ARPES and XPS measurements, the InAlAs or InGaAs layer was doped with ~10^{18} silicon atoms/cm^3 and was grown on doped InP:S (001) yielding an n-type, conductive buffer structure. Samples were then arsenic capped and transferred through air into a dedicated metals MBE system for growth of $Co_{1-x}Ni_xTiSb$. This approach was used to ensure that the same substrate structure was used for the $Co_{1-x}Ni_xTiSb$ studies. After the samples were reintroduced to ultra-high vacuum (UHV), the arsenic cap was desorbed to reveal the As-terminated (2×4) InAlAs or InGaAs surface. $Co_{1-x}Ni_xTiSb$ was grown by simultaneous evaporation of cobalt, nickel, titanium, and antimony using stoichiometric fluxes. All fluxes were measured *in-situ* using a beam flux ionization gauge calibrated by *ex-situ* Rutherford backscattering spectrometry (RBS). Samples were grown at temperatures in the range of 250-380°C as measured by a thermocouple calibrated to the arsenic desorption temperature of arsenic capped GaAs[6].

Growth of $Co_{1-x}Ni_xTiSb$ was nucleated using a thin, low temperature (250°C), seed layer, to minimize interfacial reactions. After seeding, the films were annealed and growth

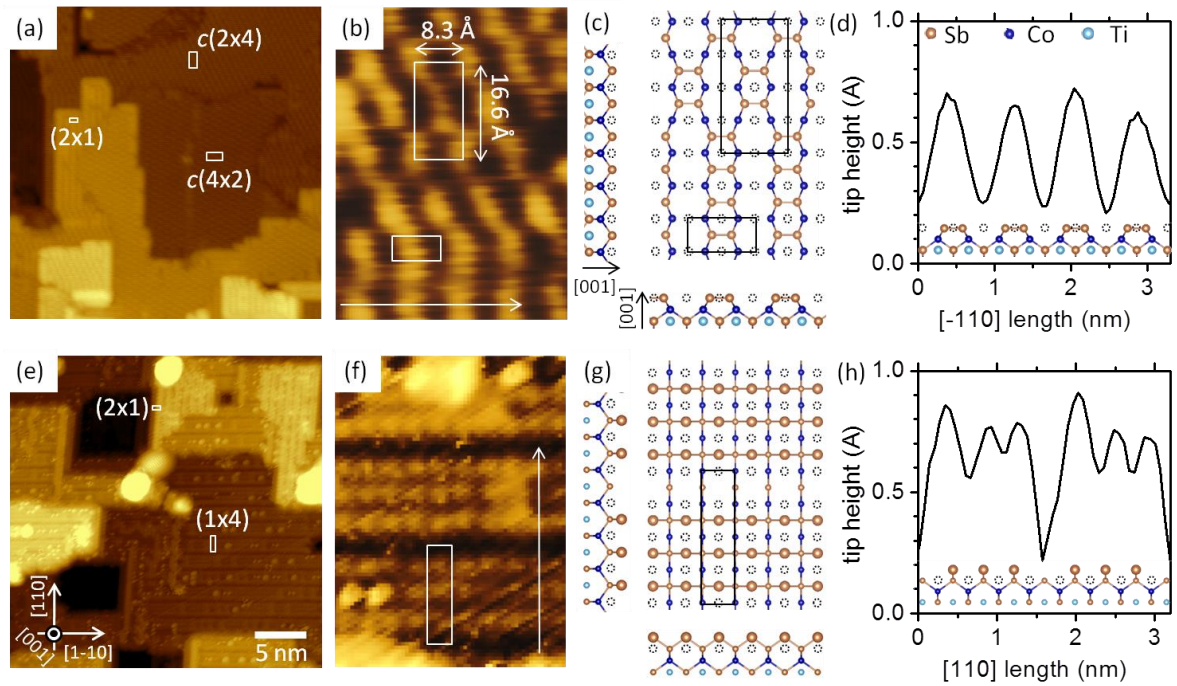

Figure 2 Filled states STM images, structure models, and tip height profiles for (a-d) the (2×1) and *c*(2×4) reconstructions and (e-h) the (1×4) reconstruction.

resumed at temperatures up to 380°C. For growth temperatures above 380°C additional spots could be observed forming on the RHEED streaks indicative of roughening, additional phase formation, or interfacial reactions. During growth, a (2x1) surface reconstruction is observed in RHEED for 50% nickel alloying or under (Figure 1(a-f)), similar to that observed in pure CoTiSb[5]. For higher levels of nickel alloying, other reconstructions including a (2x2) and disordered (3x2) (Figure 1(g-i)) are observed. These variations from the (2x1) are likely a result of the difference in the number of dangling bonds at the surface due to the additional electron per nickel atom destabilizing the (2x1) reconstruction.

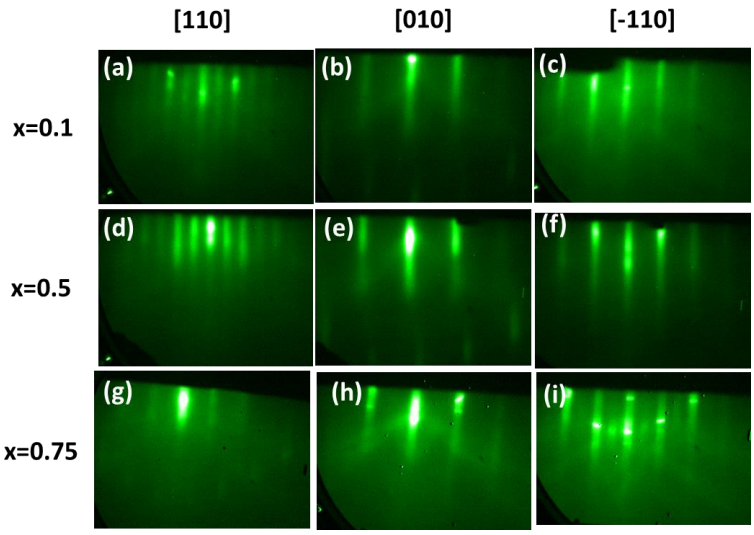

Figure 1 Reflection high energy electron diffraction (RHEED) patterns of Co1-xNixTiSb for x=0.1,0.5,0.75 along the [110], [010], and [1$\bar{1}$0] azimuths. A clear (2x1) surface reconstruction in observed for x=0.1 and 0.5, while a disordered (3x2) can be seen in x=0.75.

Figure 4(a) shows an x-ray diffraction (XRD) ω-2θ scan for 24 nm $Co_{0.5}Ni_{0.5}TiSb$ grown on InAlAs/InP(001). The sharp peaks at ω=30.44° and 63.34° correspond to the InP (002) and (004) substrate reflections, respectively, and the $Co_{0.5}Ni_{0.5}TiSb$ and InAlAs (002) and (004) peaks are nearly over- laid on the InP peaks indicating the close lattice match. Other than the (00L) peaks and thickness fringes, no additional peaks in the XRD scans are observed. Figure 4(b) shows a scan of the (004) reflection. Here finite thickness fringes can be clearly resolved with a period of Δ(2θ)=0.48 corresponding to a thickness of 23.6 nm, in good agreement with the $Co_{0.5}Ni_{0.5}TiSb$ film thickness expected from the RBS (24.0 nm). These fringes indicate a high quality interface between the $Co_{0.5}Ni_{0.5}TiSb$ and InAlAs. The large peak at 63.0°, just to the left of the substrate peak, corresponds to InAlAs with a lattice parameter of 5.89 Å. This is well lattice matched to the $Co_{0.5}Ni_{0.5}TiSb$ film (5.88 Å) and the InP substrate (5.87 Å). These XRD

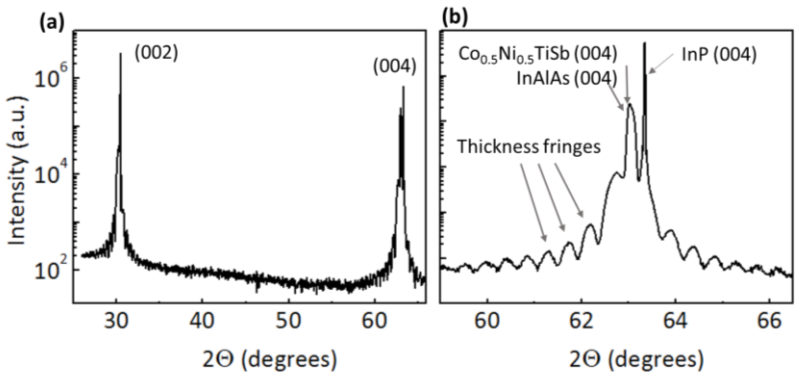

Figure 4 XRD ω-2θ scans for 24 nm $Co_{0.5}Ni_{0.5}TiSb$ grown on InAlAs/InP(001). (a) Survey scan along (00l) direction. (b) Scan of the (004) reflection.

patterns combined with the RHEED images, indicate an epitaxial cube-on-cube growth with no detectable secondary phases or orientations.

The electrical resistivity of the $Co_{1-x}Ni_xTiSb$ series was measured between 20 and 300 K using a standard dc technique in a Van der Pauw geometry by indium bonding gold wires to the samples (Figure 5(a)). All samples measured except pure NiTiSb were 24 nm of $Co_{1-x}Ni_xTiSb$ on undoped InAlAs buffers. A thin, 1 nm diffusion barrier of CoTiSb was used for the 24 nm thick NiTiSb to prevent reactions with the buffer as nickel has been previously shown to be extremely reactive with GaAs[7,8]. An approximately 5-10 nm e-beam deposited AlO_x cap was used as a protective layer to prevent oxidation of the film. Figure 5(a) shows the temperature dependent resistivity for $Co_{1-x}Ni_xTiSb$. It can be seen that for low nickel doping, the film exhibits semiconducting-like transport and thermally activated behavior. As the Ni alloying increases, the magnitude of the resistivity drops, as well as its temperature dependence until the Ni composition is greater than 25%, where metallic transport can begin to be observed.

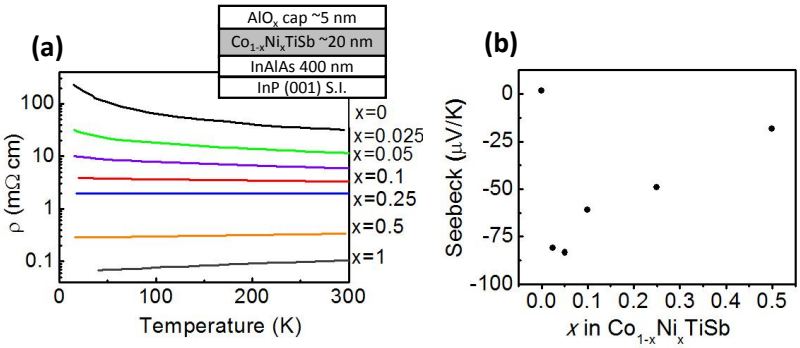

Figure 5 (a) Temperature dependent resistivity measurements for 24 nm $Co_{1-x}Ni_xTiSb$ films on InAlAs/InP (001). The sample structure can be seen in the inset. (b) Room temperature measured Seebeck coefficient for $Co_{1-x}Ni_xTiSb$ films. All films were capped with an e-beamed AlO_x layer to prevent oxidation.

The thermo-electric properties of the solid solutions were investigated. Seebeck coefficients of the series were measured at room temperature using indium soldered electrical contacts and thermal paste for the thermal probes (Figure 5(b)) Here a negative Seebeck coefficient can be observed for all levels of nickel alloying, consistent with the expectation of nickel being an electron donor. Furthermore, the magnitude of the Seebeck coefficient is largest for small amounts of Ni doping, consistent with previous results reported of vanadium alloying on the titanium site[9]. This large Seebeck coefficient for low nickel doping can be attributed to the large density of states at the Fermi level as it crosses into the conduction band, which is confirmed by the ARPES measurements discussed below.

For a better understanding of the electronic structure, ARPES measurements were performed on the series. To be able to transport samples *ex-situ* for ARPES measurements, a thin antimony capping layer was used to protect the film surface. Upon reintroduction to UHV, this capping layer was thermally desorbed. Using low-energy electron diffraction (LEED), a (3x1) reconstruction was observed upon initial antimony desorption (Figure 6(a)) for a sample temperature of 350°C, as measured by a pyrometer. This reconstruction was not previously observed in CoTiSb[10], but was confirmed to be an antimony rich reconstruction by ultraviolet photoemission spectroscopy (UPS) core levels. Upon further annealing, the observed reconstruction transformed to a mixed (2x1) and c(2x4) (Figure 6(b,c)). To examine the surface following thermal desorption of the antimony cap, scanning tunneling microscopy (STM) was performed on one of a decapped $Co_{0.25}Ni_{0.75}TiSb$ samples (Figure 6(d)). Here a well ordered surface with large steps can be observed. Moreover, both the c(2x4) seen in LEED as well as a (2x2) surface reconstruction could be resolved (Figure 6(d) insert).

ARPES measurements of (2x1)/c(2x4) $Co_{1-x}Ni_xTiSb$ films were performed at beamline I4 at the MAX-LAB synchrotron in Lund, Sweden. Measurements were conducted at 77 K to reduce the effects of thermal broadening. The final state momentum was calculated assuming free-electron-like final states where $\boldsymbol{k}_{\perp} = \sqrt{\frac{2m}{\hbar^2}(\boldsymbol{E_{Kin}} - \boldsymbol{U_0})}$ where m is the electron mass, E_{Kin} kinetic energy and the inner potential, U_o, is used as an adjustable parameter to match the periodicity of the measured bands[11]. To determine the effects of nickel doping on the band structure, normal emission ($\boldsymbol{k}_{\parallel} = \boldsymbol{0}$) scans were performed as a function of photon energy from 14 to 40 eV for a selection of compositions. Here, CoTiSb photon energies of 15 and 36 eV correspond to bulk Γ and X points, respectively. The measured normal emission energy dispersive curves (EDCs) along the Γ-Δ-X direction for pure CoTiSb and $Co_{0.5}Ni_{0.5}TiSb$ are plotted in

In the data, two types of states are observed. The first type disperses with photon energy and results from bulk states. The overlaid red line highlights the observed prominent bulk states. An additional split off band can be observed for the higher photon energies. For CoTiSb, the bulk valence band reaches a maximum of 0.6 eV below the Fermi level (binding energy = 0), in reasonable agreement with the 0.7 eV valence band edge estimated by scanning tunneling spectroscopy (STS) and XPS[10]. For $Co_{0.5}Ni_{0.5}TiSb$ a similar dispersing valence band can be observed, although the features are less prominent. Notably, intensity could be observed within the semiconducting gap of CoTiSb for all photon energies measured. However, these states have been seen previously in hard x-ray valence band photoelectron spectroscopy (HAXPES) and was attributed to in-gap states due to titanium/vacancy antisite disorder[9].

The second type of state is observed at a binding energy of approximately 0.5 eV (denoted with the dashed lines). This state does not disperse with incident photon energy (or kz), but does have in-plane (kx, ky) dispersion. Hence it is a surface state that resides within the bulk bandgap. Such a surface state was observed in films of all levels of nickel alloying and

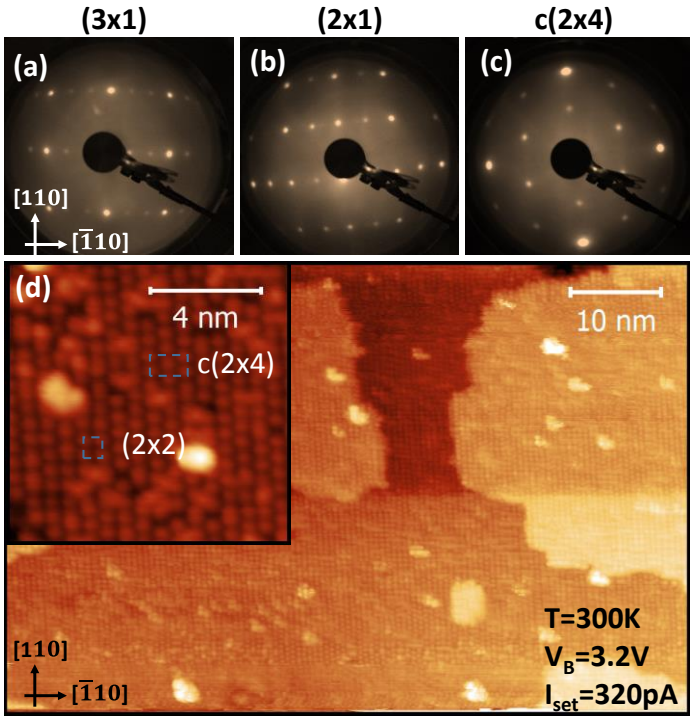

Figure 6 (a) (3x1) surface reconstructed LEED image upon initial Sb desorption with a sample temperature of 350°C. (b) (2x1) and (c) c(2x4) LEED images achieved upon further annealing with sample temperature greater than 380°C. (d) Empty states STM of decapped $Co_{0.25}Ni_{0.75}TiSb$. The inset shows an enlarged region of the scan where both c(2x4) and (2x2) surface reconstructions can be resolved. The surface unit cells are enclosed in the dashed boxes.

was previously investigated for CoTiSb[10]. For the highest levels of Ni alloying, an additional surface state could be observed near the Fermi level.

Figure 7(c) and (d) show valence band spectra at the bulk X (36 eV) and Γ (15 eV) points, respectively for five of the compositions measured. At the bulk X-point we can observe a state just below the Fermi level for films with >10% nickel alloying. This state corresponds to the appearance of the conduction band. For the 10% alloyed film a shoulder is observable at the Fermi level in the spectrum, indicating that the position of the Fermi level is near the conduction band edge. This is in good agreement with the semiconductor to metal transition observed in temperature dependent resistivity measurements. Additionally, we observe that the position of the valence bands and surface state generally shift to higher binding energies. These results are consistent with a rigid band shift due to the Fermi level moving to higher energies due to the added electrons from the nickel atoms.

Beyond nickel content, the annealing conditions influence the position and intensity of the observed bands. Figure 8(a) and (b) show the normal emission EDCs for the antimony rich (3x1) and higher temperature annealed c(2x4) surface reconstructions. Here similar bulk valence band and surface state features are observed with two notable departures. Both the bulk valence band and, in particular, the surface state become more pronounced for the higher

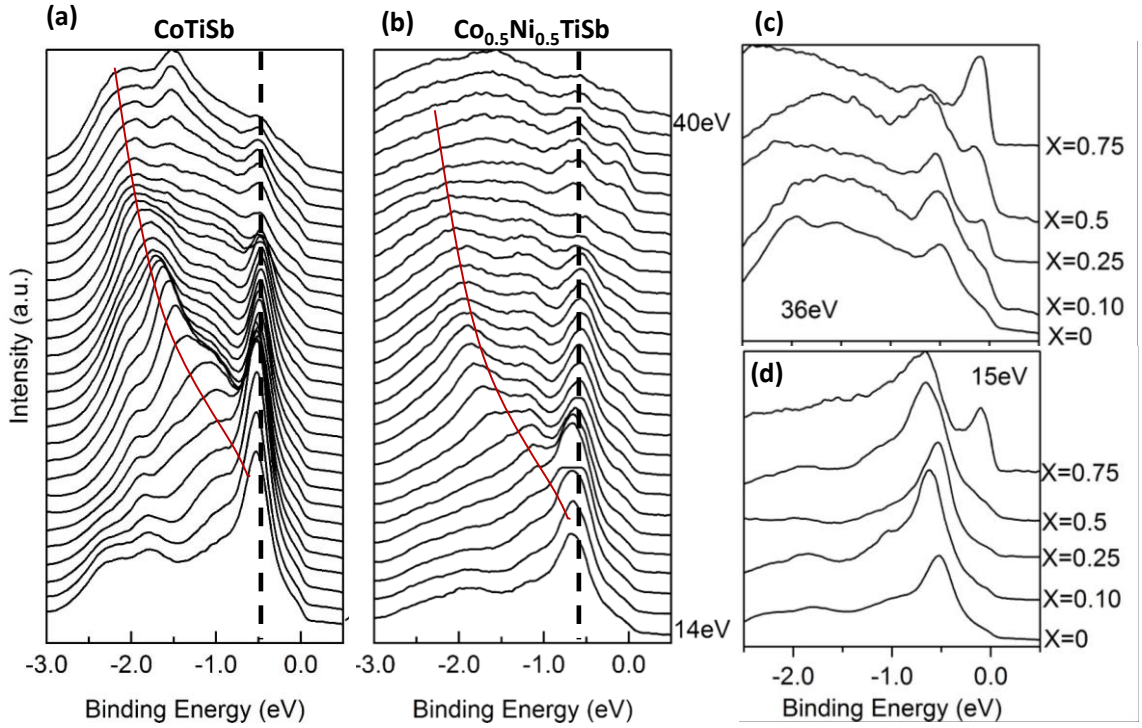

Figure 7 Series of valence-band photoemission spectra normal to the (001) surface plane from 14 eV to 39 eV which corresponds to the Γ-Δ-X direction for (a) CoTiSb and (b)$Co_{0.5}Ni_{0.5}TiSb$ films. The dispersive state corresponding to the valence band has been highlighted by the red line. The non-dispersive state near 0.5eV binding energy corresponds to a surface state seen in all films measured. Valence band spectra at the bulk (c) X (36 eV) and (d) Γ (15 eV) points respectively for five of the compositions measured.

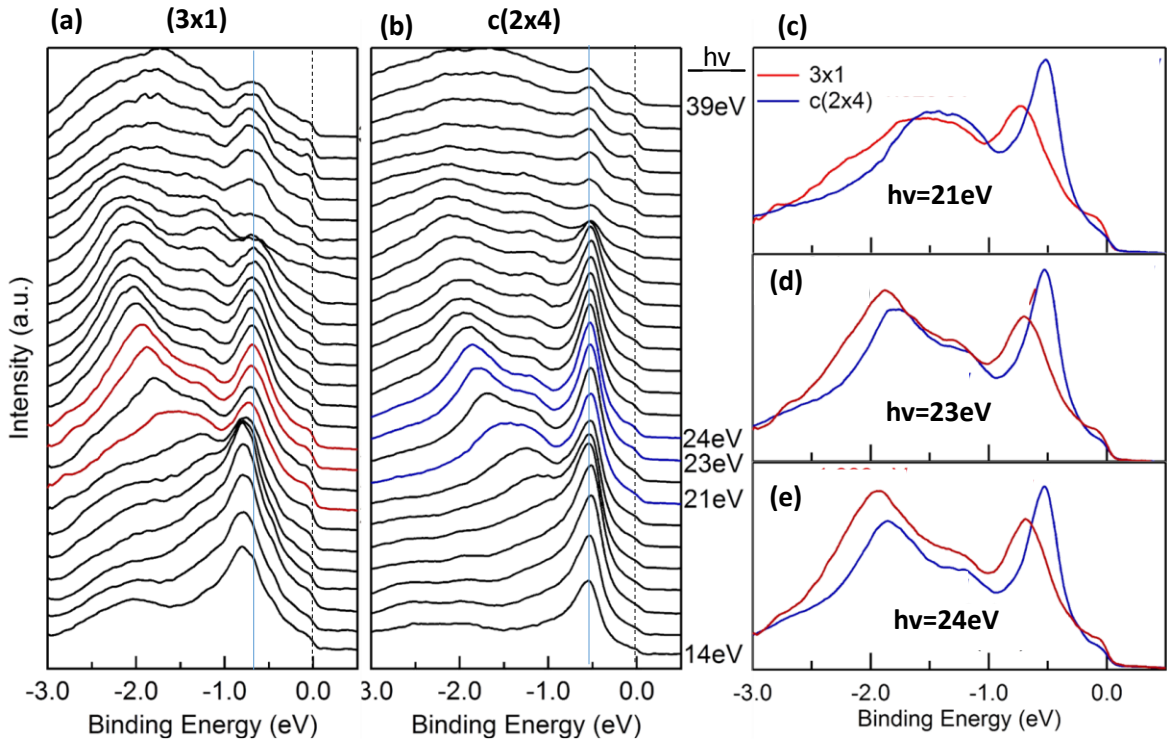

Figure 8 Energy dispersion curves as a function of incident photon energy from 14 to 39 eV for $Co_{0.25}Ni_{0.75}TiSb(001)$, which probes along the Γ-Δ-X direction of the bulk Brillouin zone for (a) the antimony rich (3x1) and (b) further annealed c(2x4) surface reconstructions. (c-e) EDC's measured in normal emission on the two surface reconstructions of $Co_{0.25}Ni_{0.75}TiSb$ for 21, 23, and 24 eV highlighting the shift in the bands by 0.2 eV to lower binding energy for the higher temperature annealed surface, c(2x4).

temperature annealed condition. The increase in band clarity is likely due to the excess antimony on the (3x1) reconstruction attenuating intensity from the underlying surface and upon further desorption, the surface bands become sharper. This would suggest the observed surface state originates from antimony dimerization or surface antimony bonding with the bulk. This is consistent with previous ARPES on CoTiSb[10] and XPS core levels from PtLuSb[12].

Band Alignments between CoTiSb and InGaAs, InAlAs and NiTiSn

To determine the band lineup of CoTiSb with conventional III/V's, the valence-band discontinuities in abrupt CoTiSb/InGaAs(001) and CoTiSb/InAlAs(001) heterojunctions were determined using XPS *in-situ* using monochromated Al Kα radiation (hν = 1486.3 eV). This method uses the energy difference of the core level (CL) to valence band edge (VBE) as a means of accurately measuring heterojunction band discontinuities[13]. The valence band offset (ΔE_v) can be observed when a 1 nm over layer of the second material is deposited on the first. The effective photoelectron escape depth λ for x-rays is ~1-2nm; thus photoelectrons originating from both sides of the heterojunction interface will be collected.

All samples were grown using MBE and transferred *in-situ* to the XPS for collection of the spectra. Bulk spectra were collected from 400+nm thick InAlAs and InGaAs and 15+ nm CoTiSb samples. 1-3 nm films were deposited for the heterojunction spectra. The heterojunctions measured include CoTiSb/InAlAs, CoTiSb/InGaAs, and InGaAs/CoTiSb. The cobalt 3p (BE~60eV), aluminum 2p (BE~74eV), indium 3d (~19eV), and gallium 3d (~21eV) core levels were used to calculate the valence band offsets. In Figure 9 (a-c) XPS spectra for (a) cobalt 3p core level and VBE from a 16nm thick CoTiSb film, (b) aluminum 2p core level and VBE from a 470nm thick InAlAs film, and (c) aluminum 2p and cobalt 3p CLs from a 1 nm thick CoTiSb/InAlAs interface. The indium core level position of InAlAs was also measured and included in the calculation of ΔE_v. Beyond the CoTiSb/InAlAs heterointerface, both the CoTiSb/InGaAs and InGaAs/CoTiSb heterointerfaces were also measured using the same procedure discussed above (plots not shown). Particular care was taken fitting the indium and gallium core level positions because they are only separated by ~2eV. The results are schematically shown in a band alignment diagram in Figure 9(d) Here, the reported ΔE_v for CoTiSb/InGaAs alignment averages the CoTiSb on InGaAs (ΔE_v=0.31±0.05) and InGaAs on CoTiSb (ΔE_v=0.33±0.05) results. Therefore the CoTiSb/InGaAs heterointerface satisfies transitivity within the experimental error of our setup. From these measurements we deduce that CoTiSb has a type I and type II band alignment with InAlAs and InGaAs respectively.

Most recently, we have begun investigating the effects of substitutionally alloying cobalt for nickel in NiTiSn as well as the properties of CoTiSb/NiTiSn heterojunctions. Here, cobalt has one less electron than nickel, thus is a hole donor in cobalt doped NiTiSn films. The

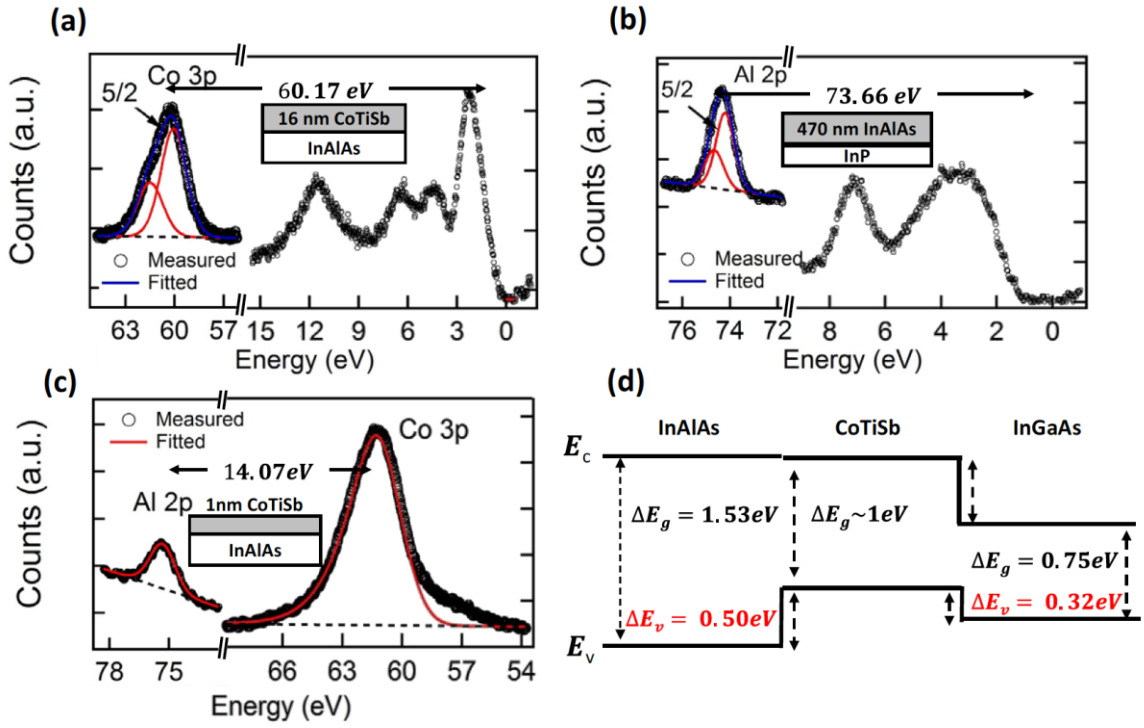

Figure 9 Band offsets using XPS: spectra of (a) cobalt 3p core level and valence band edge (VBE) from a 16nm thick CoTiSb film, (b) aluminum 2p core level and VBE from a 470nm thick InAlAs film, (c) aluminum 2p and cobalt 3p core levels from a 1 nm thick CoTiSb/InAlAs interface, and (d) energy-band alignment of the InAlAs/CoTiSb/InGaAs heterointerfaces, respectively.

Seebeck coefficient for 20nm $Ni_{1-x}Co_xTiSn$ films grown on MgO (001) is displayed in Figure 10(a). Here we can see a crossover from n-type (electron) to p-type (hole) conduction for low levels of cobalt alloying verifying that cobalt is a hole donor. Future work will examine the properties of these films in more detail, including temperature dependent transport, magnetism, and structural properties. Additionally, CoTiSb/NiTiSn heterojunctions have been successfully grown and characterization begun. Figure 10(b) shows a ω-2θ x-ray diffraction scan of the CoTiSb/NiTiSn (004) reflection. There is clear observable diffraction peak intensity from both films at their relaxed lattice constants of 5.88Å and 5.94Å for CoTiSb and NiTiSn, respectively. Future work will examine the valence-band offsets between CoTiSb and NiTiSn as well as the vertical and in-plane transport properties of these heterojunctions.

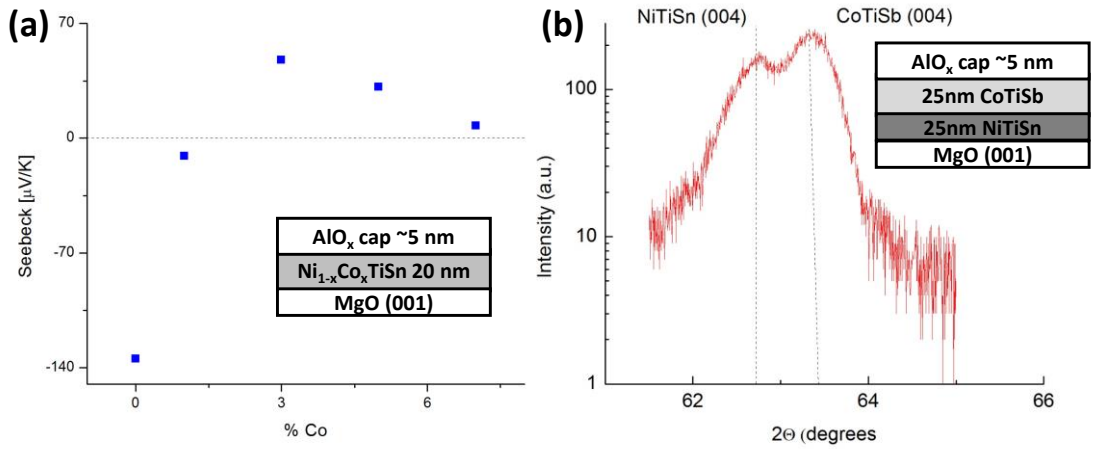

Figure 10 (a) Seebeck coefficient for $Ni_{1-x}Co_xTiSn$ films for low levels of cobalt alloying. (b) XRD scan of the (004) reflection of a CoTiSb/NiTiSn/MgO(001) heterostructure.

PtLuSb – Predicted Topological Materials Studies

Finally, the electronic structure of the half Heusler compound PtLuSb (001) was studied using ARPES[14]. At equilibrium, PtLuSb is predicted to lie at the border between normal and inverted band ordering[15,16] with a topologically insulating band structure. If experimentally realizable, this would provide an opportunity for the creation of entirely new heterostructure spintronic devices that make use of the structurally-identical but electronically-varied nature of Heusler compounds as well as to potentially enable the discovery of new materials with electronic structures such as topological superconductors (of interest for spintronic and quantum computing applications).

In agreement with theory calculations, previous experimental studies for bulk single crystals[17,18] and thin-films[12] have confirmed that PtLuSb has the expected zero-gap band-structure but have not measured the momentum resolved electronic band structure. To do so, samples were grown by MBE beginning with an 5ML GdSb / $Al_{0.1}In_{0.9}Sb$:Be / p-GaAs (001) buffer layer structure. After an in-situ transfer, growth was continued with a 20nm PtLuSb layer and a 200nm antimony sacrificial capping layer. The combination of the GdSb diffusion barrier and antimony capping layer enables the completed samples to be transferred *ex-situ* for

ARPES measurements without the PtLuSb oxidizing and then allows the residual antimony to be thermally desorbed. Without the GdSb layer, interfacial reactions occur between the $Al_{0.1}In_{0.9}Sb$ and PtLuSb prior to complete desorption of the antimony cap.

Three main elements are needed to confirm identification of a topological surface state: first, the state must be confined and show no out-of-plane dispersion; second, the state should be linearly dispersing with a Dirac-like in-plane dispersion; and third, spin-momentum locking should be evident[19]. Examining the out-of-plane dispersion maps (Figure 11(a)) we note an absence of k_z dispersion, consistent with the behavior of a surface state. Furthermore, by tracking this surface state through binding energy (Figure 11(b)), we observe a linear in-plane dispersion reminiscent of the bottom half of a Dirac cone. Lastly, if we examine spin-ARPES measurements of the left and right sides of this Dirac-like surface state (Figure 11(d,e) and (f,g), respectively), we note a distinct opposing spin polarization. By correlating the observed spin polarizations with the detector geometry, we find that a strong counter-clockwise helical spin texture is present, similar to that seen in Bi_2Se_3[20]. Consequently, the observed behavior meets all three criteria for a topological surface state, confirming the accuracy of the prior

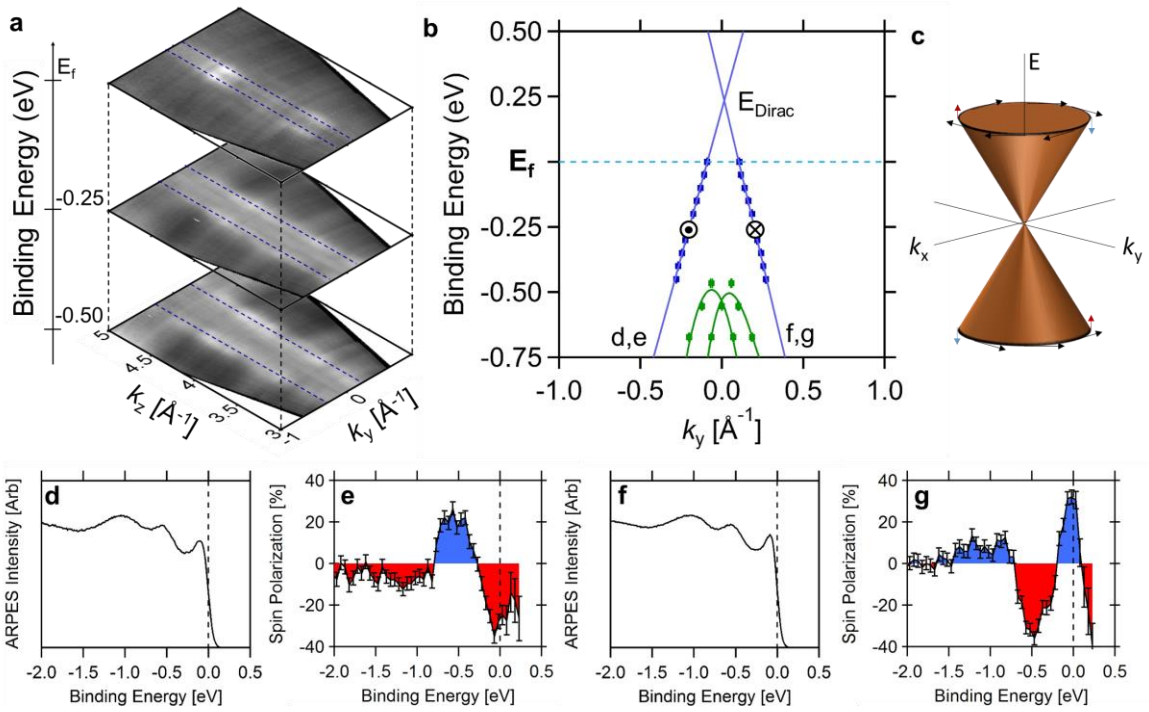

Figure 11 (a) Out-of-plane momentum dependence for various binding energies. An absence of kz dispersion is observed, consistent with the behavior of a surface state. (b) By tracking this state's position as a function of binding energy, a Dirac-like behavior can be see with a crossing point approximately 235 meV above the Fermi level. Spin-ARPES spin polarization directions are marked. (c) Schematic diagram of a topological surface state with helical spin texture. (d-e,f-g) ARPES intensity and corresponding spin polarization for the left and right side of the linearly dispersing surface state, respectively. A counter-clockwise helical spin texture, consistent with theory, is observed. Furthermore, a Rashba-like split hole band can be seen at lower binding energies.

theory calculations and highlighting the multifunctional nature of Heusler compounds by demonstrating the presence of another unique electronic structure.

Conclusions

In summary, the growth and electronic properties of the solid solution series $Co_{1-x}Ni_xTiSb$ was investigated. For low levels of nickel alloying the (2x1) surface reconstruction observed in pure CoTiSb persisted. However, for higher levels of nickel alloying new surface reconstructions including a (2x2) and disordered (3x2) were observed. In electrical resistivity, a slow transition from semiconductor to metallic behavior was observed for moderate levels of nickel alloying (>10% nickel). ARPES measurements support that the Fermi level crosses the conduction band edge beyond 10% nickel alloying. Furthermore, the surface reconstruction and annealing temperature influence the Fermi level pinning position by changing the strength of surface induced band bending. The valence band offset of the CoTiSb/InAlAs and CoTiSb/InGaAs heterointerfaces were determined to be ΔE_v=0.50 and ΔE_v=0.32, respectively. $Ni_{1-x}Co_xTiSb$ films demonstrate the carrier type and thermoelectric properties of NiTiSn can be tuned by cobalt alloying. CoTiSb/NiTiSn half Heusler heterostructures have successfully been grown, which represent the first MBE demonstration of a semiconductor half-Heusler/half-Heusler heterostructure. Finally, APRES and spin-ARPES results of predicted topological insulator PtLuSb have confirmed the presence of a topologically non-trivial surface state in agreement with theory calculations.

References

[1] H. Kandpal, C. Felser, and R. Seshadri, J. Phys. D. Appl. Phys. **39**, 776 (2006).

[2] M. Katsnelson, V. Irkhin, L. Chioncel, a. Lichtenstein, and R. de Groot, Rev. Mod. Phys. **80**, 315 (2008).

[3] S. Chen and Z. Ren, Mater. Today **16**, 387 (2013).

[4] H. Lin, L.A. Wray, Y. Xia, S. Xu, S. Jia, R. Cava, A. Bansil, and M. Hasan, Nat. Mater. **9**, 546 (2010).

[5] J.K. Kawasaki, L.I.M. Johansson, B.D. Schultz, and C.J. Palmstrøm, Appl. Phys. Lett. **104**, 022109 (2014).

[6] U. Resch, N. Esser, Y. Raptis, and W. Richter, Surf. Sci. (1992).

[7] M. Ogawa, Thin Solid Films **70**, 181 (1980).

[8] S.H. Chen, C.B. Carter, C.J. Palmstrøm, and T. Ohashi, Appl. Phys. Lett. **48**, 803 (1986).

[9] S. Ouardi, G. Fecher, C. Felser, and M. Schwall, Phys. Rev. B **86**, 045116 (2012).

[10] J.K. Kawasaki, A. Janotti, L.I.M. Johansson, M. Hjort, A. Mikkelsen, B. Thiagarajan, B.D. Schultz, and C.J. Palmstrøm, [Unpublished] (n.d.).

[11] S. Hufner, *Photoemission Spectroscopy: Principles and Applications 3rd Ed.* (2003).

[12] S.J. Patel, J.K. Kawasaki, J. Logan, B.D. Schultz, J. Adell, B. Thiagarajan, A. Mikkelsen, and C.J. Palmstrøm, Appl. Phys. Lett. **104**, 201603 (2014).

[13] E.A. Kraut, R.W. Grant, J.R. Waldrop, and S.P. Kowalczyk, Phys. Rev. Lett. **44**, 1620 (1980).

[14] J.A. Logan, S.J. Patel, S.D. Harrington, C.M. Polley, B.D. Schultz, B. Thiagarajan, A. Janotti, A. Mikkelsen, and C.J. Palmstrøm, Nat. Mater. (2015).

[15] W. Al-Sawai, H. Lin, R. Markiewicz, L.A. Wray, Y. Xia, S.-Y. Xu, M.Z. Hasan, and A. Bansil, Phys. Rev. B **82**, 125208 (2010).

[16] S. Chadov, X. Qi, J. Kübler, G. Fecher, C. Felser, and S.-C. Zhang, Nat. Mater. **9**, 541 (2010).

[17] C. Shekhar, S. Ouardi, G.H. Fecher, A. Kumar Nayak, C. Felser, and E. Ikenaga, Appl. Phys. Lett. **100**, 252109 (2012).

[18] Z. Hou, Y. Wang, G. Xu, X. Zhang, E. Liu, W. Wang, Z. Liu, X. Xi, W. Wang, and G. Wu, **102102**, (2015).

[19] Y. Ando, J. Phys. Soc. Japan **82**, 102001 (2013).

[20] Y. Xia, D. Qian, D. Hsieh, L. Wray, A. Pal, H. Lin, A. Bansil, D. Grauer, Y.S. Hor, R.J. Cava, and M.Z. Hasan, Nat. Phys. **5**, 398 (2009).